The Astrophysical Journal Supplement Series, 271:14 (10pp), 2024 March https://doi.org/10.3847/1538-4365/ad1877

Near-real-time 3D Reconstruction of the Solar Coronal Parameters Based on the Magnetohydrodynamic Algorithm outside a Sphere Using Deep Learning

Sumiaya Rahman[1], Hyun-Jin Jeong[2], Ashraf Siddique[3], Yong-Jae Moon[1,2], and Bendict Lawrance[2]
[1] School of Space Research, Kyung Hee University, Yongin, 17104, Republic of Korea; moonyj@khu.ac.kr
[2] Department of Astronomy and Space Science, Kyung Hee University, Yongin, 17104, Republic of Korea
[3] Department of Computer Science Engineering, Kyung Hee University, Yongin, 17104, Republic of Korea
Received 2023 August 13; revised 2023 December 5; accepted 2023 December 22; published 2024 February 21

Abstract

For the first time, we generate solar coronal parameters (density, magnetic field, radial velocity, and temperature) on a near-real-time basis by deep learning. For this, we apply the Pix2PixCC deep-learning model to three-dimensional (3D) distributions of these parameters: synoptic maps of the photospheric magnetic field as an input and the magnetohydrodynamic algorithm outside a sphere (MAS) results as an output. To generate the 3D structure of the solar coronal parameters from 1 to 30 solar radii, we train and evaluate 152 distinct deep-learning models. For each parameter, we consider the data of 169 Carrington rotations from 2010 June to 2023 February: 132 for training and 37 for testing. The key findings of our study are as follows: First, our deep-learning models successfully reconstruct the 3D distributions of coronal parameters from 1 to 30 solar radii with an average correlation coefficient of 0.98. Second, during the solar active and quiet periods, the AI-generated data exhibits consistency with the target MAS simulation data. Third, our deep-learning models for each parameter took a remarkably short time (about 16 s for each parameter) to generate the results with an NVIDIA Titan XP GPU. As the MAS simulation is a regularization model, we may significantly reduce the simulation time by using our results as an initial configuration to obtain an equilibrium condition. We hope that the generated 3D solar coronal parameters can be used for the near-real-time forecasting of heliospheric propagation of solar eruptions.

Unified Astronomy Thesaurus concepts: Active solar corona (1988); Astronomy data analysis (1858); Astronomy image processing (2306); The Sun (1693)

1. Introduction

The solar coronal parameters such as density, magnetic field, radial velocity, and temperature are fundamental variables for describing the physical processes that occur in the solar corona and the inner heliosphere. In fact, those parameters have a dominant influence on the dynamics, structures, and evolutionary phenomena observed in the solar atmosphere, particle accelerations, and propagation. These coronal parameters characterize the overall structure of the solar corona and the position of the heliospheric current sheet, influence the regions of fast and slow solar wind, and predict the probable locations of coronal mass ejections (Linker 1998). Ultimately, these solar coronal parameters control the evolution of physical phenomena in the solar system, including the Sun itself and the disastrous space weather events in the solar–terrestrial and interplanetary space environment (Tan 2022). The magnetohydrodynamic algorithm outside a sphere (MAS; Linker et al. 1999; Mikić et al. 1999) model allows us to determine the large-scale structure of the magnetic field in the corona, along with the distribution of the solar wind velocity, plasma density, and temperature. It is a 3D magnetohydrodynamic (MHD) simulation model that is built using computational physics and solar corona modeling, and it covers from 1 to 30 solar radii and the inner heliosphere from 30 solar radii to 5 au. The MAS model, being a time-dependent resistive polytropic MHD model, utilizes suitable boundary conditions and advances the MHD equations forward in time (Riley et al. 2011). Typically, the implementation of this resistive MHD model involves significant preprocessing and postprocessing. Moreover, due to user time and queue limits at computer centers, running the MAS code with high spatial resolution and long-duration evolution parameters may necessitate additional computational resources (Caplan et al. 2019).

Generative adversarial network (GAN; Goodfellow et al. 2014) models are widely used for structured data, particularly in tasks such as image translation. The Pix2Pix (Isola et al. 2017) and the Pix2PixHD (Wang et al. 2018) are supervised models based on a GAN. Those models have been applied in various areas of astronomy and space weather applications: (1) image translation among mutiwavelength images (Kim et al. 2019; Park et al. 2019; Jeong et al. 2020; Shin et al. 2020; Jeong et al. 2022; Lawrance et al. 2022), (2) denoising the solar magnetogram (Park et al. 2020), (3) superresolution of the solar data (Jia et al. 2019; Rahman et al. 2020), and (4) the 3D reconstruction of coronal electron density (Jang et al. 2021; Rahman et al. 2023).

In our previous paper (Rahman et al. 2023), we successfully produced a 3D density structure of the solar corona from 1 to 30 solar radii using the Pix2PixHD model (Wang et al. 2018) whose computing time was much shorter than the MAS simulation. The synthetic coronagraphic data estimated from the results are consistent with the real coronagraph image of the Solar Heliospheric Observatory/Large Angle Spectroscopic Coronagraph C3 coronagraph data. Following Rahman et al. (2023), we generate solar coronal parameters (magnetic field, radial velocity, and temperature) at a near-real-time basis using the Pix2PixCC model. Along with the density results, the AI-generated 3D structure of the solar coronal magnetic field, radial velocity, and temperature from our Pix2PixCC models can be employed for the inner boundary conditions for heliospheric simulation models such as the MAS heliospheric

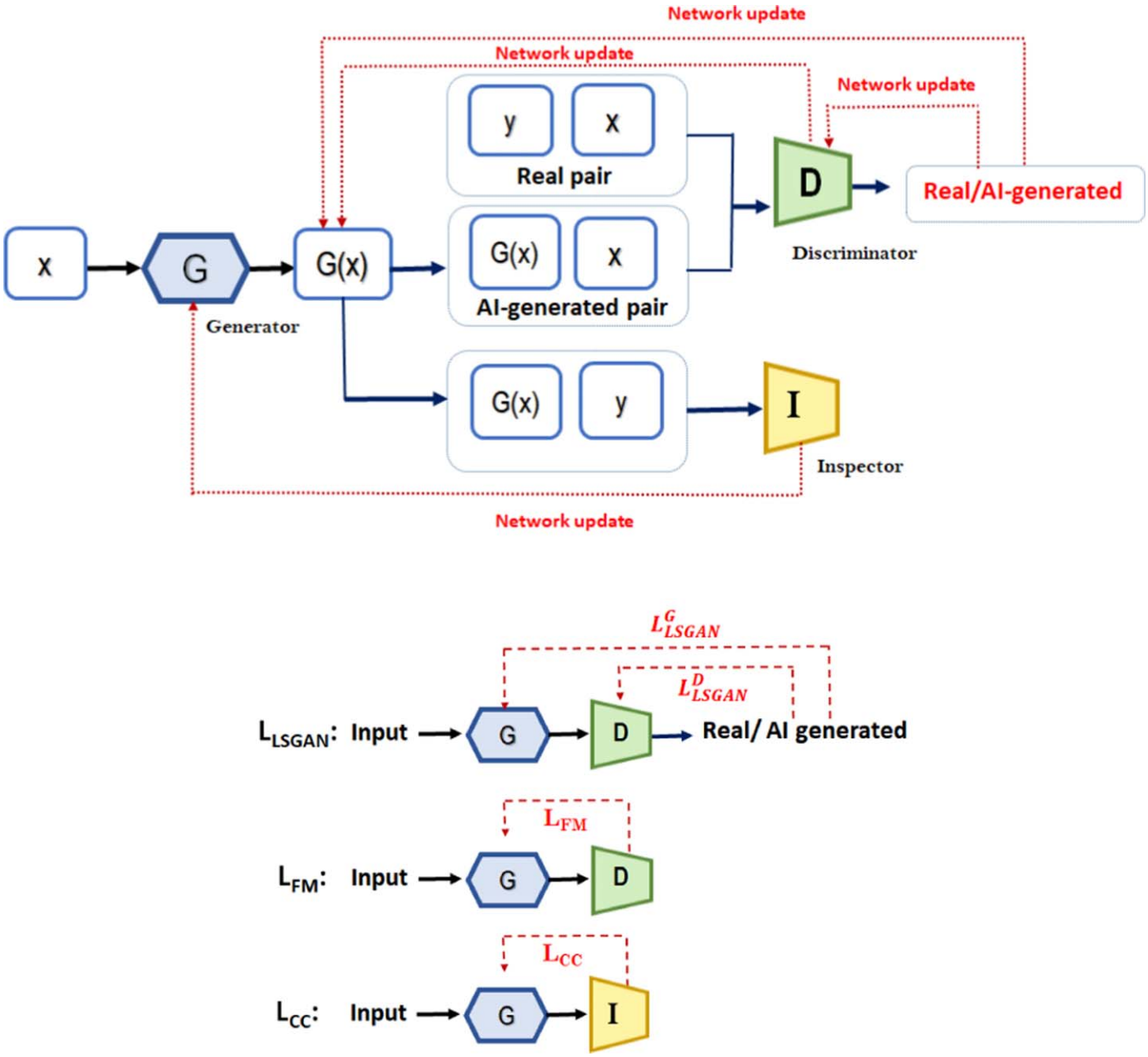

Figure 1. The flowchart of the Pix2PixCC model and the loss functions.

models (Lionello et al. 2009) and the Wang–Sheeley–Arge model (Arge et al. 2004).

The paper is organized as follows. The data and the methods of the Pix2PixCC model are described in Sections 2 and 3. The results and discussions are given in Section 4. The summary of our study is given in Section 5.

2. Data

The MAS simulation model, developed by CORHEL (for CORona-HELiosphere), is a suite of models and tools dedicated to modeling the solar corona and inner heliosphere. CORHEL delivers solutions to the community via Predictive Science Inc. (PSI). The PSI coronal code MAS solves time-dependent MHD equations until a steady state is reached, with the boundary condition defined by a magnetic map (Linker 2011). For this study, we collected the solar coronal parameter data of 169 Carrington rotations (CRs) from 2010 June to 2023 February for training and testing. We took the data regarding these parameters from the PSI website.[4] Following our previous work (Rahman et al. 2023), we incorporate data augmentation techniques to enhance the amount of data. These provide diversity into the data set during the training process and help to address potential artifact issues during testing (Shorten & Khoshgoftaar 2019). After the data augmentation, the number of training data sets increases from 132 to 9504 for each parameter. The data augmentation is not applied to the test data sets.

We train the deep-learning models using the synoptic maps of the photospheric magnetic field as input data to generate the 3D solar coronal parameters (magnetic field, radial velocity,

[4] http://www.predsci.com/data

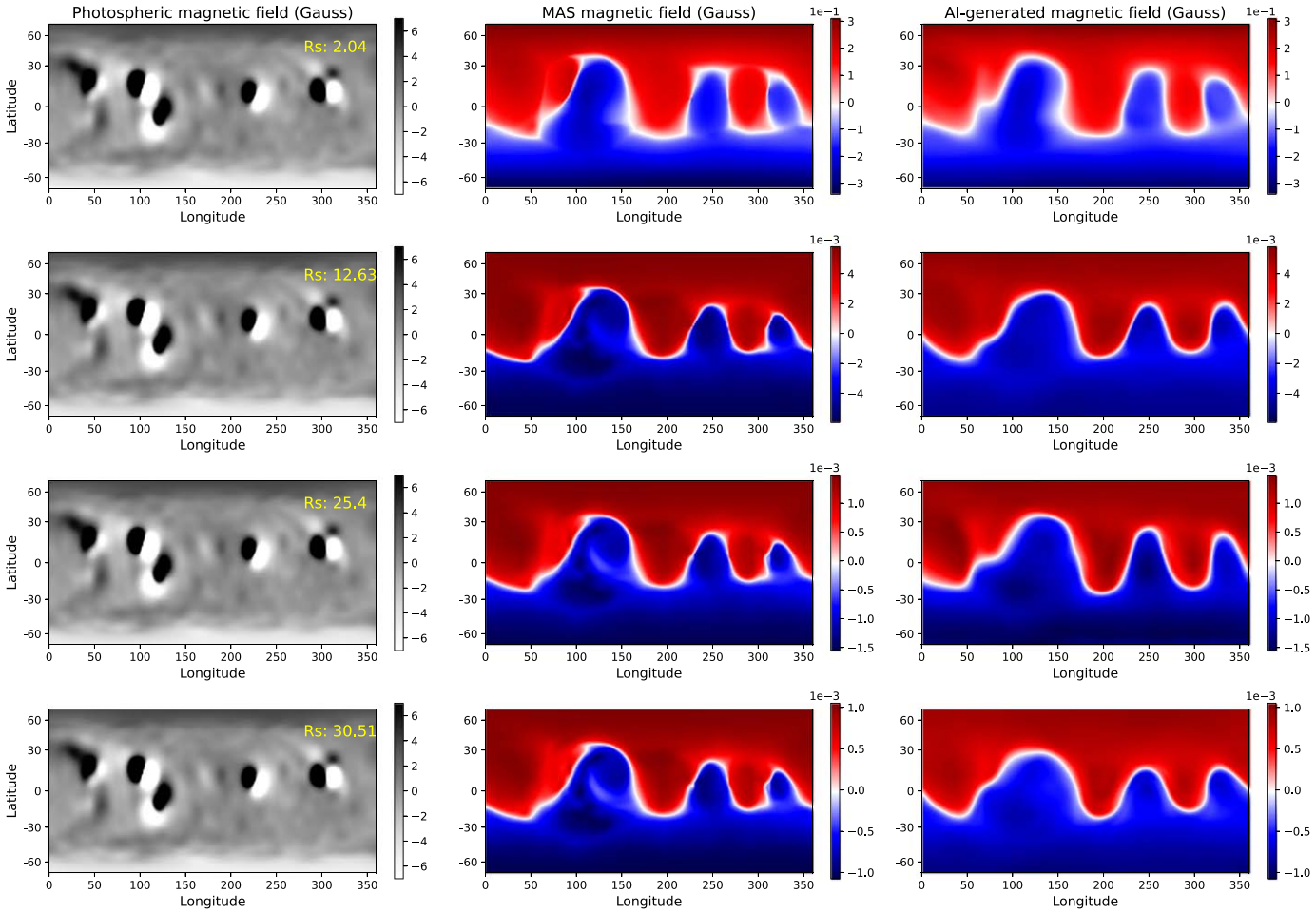

Figure 2. Visual comparisons of the solar coronal magnetic field structure between the MAS simulation results and AI-generated during CR 2194 at 2.04, 12.63, 25.40, and 30.51 solar radii, respectively. Left column: synoptic map of the photospheric magnetic field. Middle column: the magnetic field maps from the MAS simulation model. Right column: AI-generated ones.

and temperature) as target data from 1 to 30 solar radii. We employ an interpolation technique that considers the latitude and longitude position for the alignment of the parameters. By considering the distances between neighboring latitude and longitude positions, we interpolate both the input and the target. The size of our input and target data sets are 182×101 (longitude, latitude) and $182 \times 101 \times 150$ (longitude, latitude, and altitude from the solar surface), respectively. We also normalize the data sets according to Rahman et al. (2023). For analyzing the results of the test data sets, we denormalized and converted the MAS code units to cgs units, following the process described in Mikić et al. (2018).

3. Method

Following our previous study (Rahman et al. 2023), in this study we apply the deep-learning model Pix2PixCC (Jeong et al. 2022) which is an improved model of Pix2PixHD, to generate the major solar coronal parameters (magnetic field, radial velocity, and temperature) from the photospheric magnetic field. Jeong et al. (2022) showed that they improved the generation of synthetic solar farside magnetograms from Solar Terrestrial Relations Observatory (Kaiser et al. 2008) and Solar Dynamics Observatory (Pesnell et al. 2012) data sets using the Pix2PixCC model. Along with the generator (G) and the discriminator (D), the Pix2PixCC model incorporates an additional component called the inspector (I). The generative network is composed of several convolutional layers and transposed convolutional layers. A convolutional layer automatically extracts features from the input data, while a transposed convolutional layer attempts to reconstruct the output using the extracted features. The discriminator (D) is constructed using multiple convolutional layers. It incorporates two specific loss functions: the feature matching (FM) loss and the least-squares GAN (LSGAN) loss (Mao et al. 2016). The FM loss optimizes the parameters of the generator based on the generated feature map by convolution layers. On the other hand, the LSGAN penalizes the fake samples and pushes the generator to produce outputs that are closer to the decision boundary, making them more realistic.

The objective function of loss functions can be represented as follows:

$$\mathcal{L}_{\mathrm{FM}}(G, D) = \sum_{i=1}^{T} \frac{1}{N_i} \| [D^{(i)}(x, y) - D^{(i)}(x, G(x))] \|, \quad (1)$$

$$\mathcal{L}^{D}_{\mathrm{LSGAN}}(G, D) = \frac{1}{2}[(D(x, y) - y)^2] + \frac{1}{2}[(D(x, G(x)))^2], \quad (2)$$

$$\mathcal{L}^{G}_{\mathrm{LSGAN}}(G, D) = \frac{1}{2}[(D(x, G(x) - y)^2], \quad (3)$$

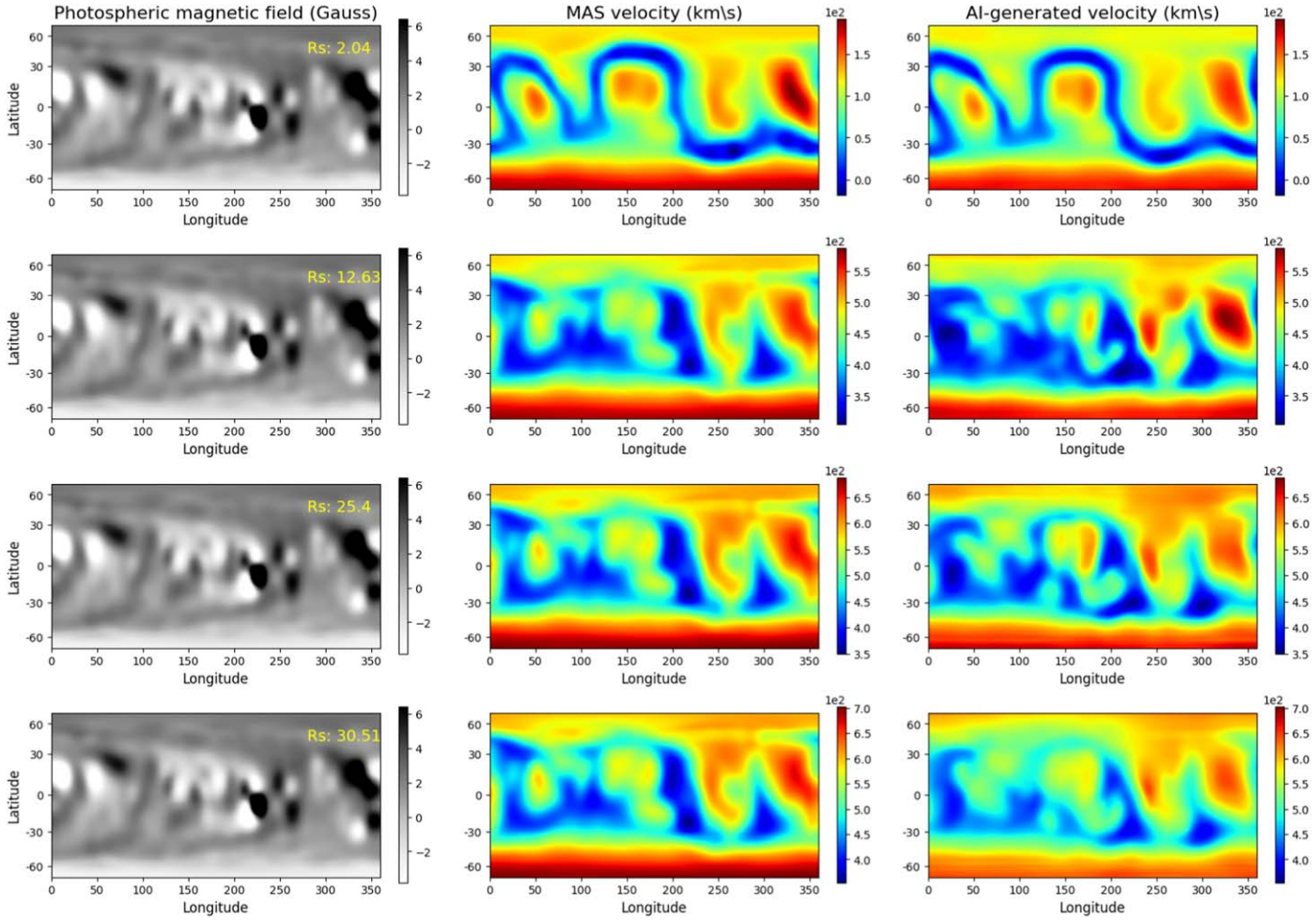

Figure 3. Comparisons of the solar coronal radial velocity map between the MAS simulation results and AI-generated ones on CR 2178 at 2.04, 12.63, 25.40, and 30.51 solar radii, respectively. Left column: synoptic map of the photospheric magnetic field. Middle column: the radial velocity maps from the MAS simulation model. Right column: AI-generated ones.

where x and y denote the input (photospheric magnetic field) and target (magnetic field, radial velocity, and temperature) data, respectively. T, N_i denotes the total number of convolution layers in the discriminator, and the number of pixels in the feature maps from a convolution layer. $G(x)$ is the generated output. $D(x, y)$ and $D(x, G(x))$ are probabilities of the real and AI-generated pairs.

The inspector (I) tries to stabilize the training of the generator by applying an additional correlation coefficient (CC) loss function. It is based on Lin's concordance CC, which measures the degree to which pairs of data points align with the 45° line passing through the origin. It is shown that the Pix2PixCC model with this CC-based loss function has better performance for large-dynamic-range data (Jeong et al. 2022) than Pix2PixHD. The CC loss function is defined as

$$\mathcal{L}_{\mathrm{CC}}(G) = \sum_{i=0}^{T} \frac{1}{T+1}[(1 - \mathrm{CC}_i(y, G(x))], \tag{4}$$

where T is the total number of downsampling by a factor of 2 and i is the number of downsampling, respectively. The CC value between 2^i times the downsampled target and AI-generated data is represented by CC_i.

Figure 1 represents the overall model and the loss function architectures. In both training and testing processes, the photospheric magnetic field (x) is provided as an input to the deep-learning models. The generator aims to generate the MAS simulation–like 3D magnetic field, radial velocity, and temperature map $G(x)$ from inputs and then provides $G(x)$ data to the discriminator and the inspector. The discriminator differentiates between the AI-generated pair ($G(x)$, x) and real pair (y, x), and the inspector calculates CCs between the target y and $G(x)$.

The final objective of the Pix2PixCC is as follows:

$$\min_G \lambda_1 \mathcal{L}^G_{\mathrm{LSGAN}}(G, D) + \lambda_2 \mathcal{L}_{\mathrm{FM}}(G, D) + \lambda_3 \mathcal{L}_{\mathrm{CC}}(G, D), \tag{5}$$

$$\min_D \mathcal{L}^D_{\mathrm{LSGAN}}(G, D), \tag{6}$$

where λ_1, λ_2, and λ_3 are hyperparameters that assigned the weights to $\mathcal{L}_{\mathrm{LSGAN}}$, $\mathcal{L}_{\mathrm{FM}}$, and $\mathcal{L}_{\mathrm{CC}}$, respectively. The values are given as 2 for λ_1, 10 for λ_2, and 5 for λ_3.

To obtain the 3D structure of the parameters across the range of 1–30 solar radii, we train a total of 152 deep-learning models for 152 solar radii separately for each parameter. During the training process, we get best results for the magnetic field and radial velocity at epoch 10,000, while for the temperature, the best results are achieved at epoch 300. The

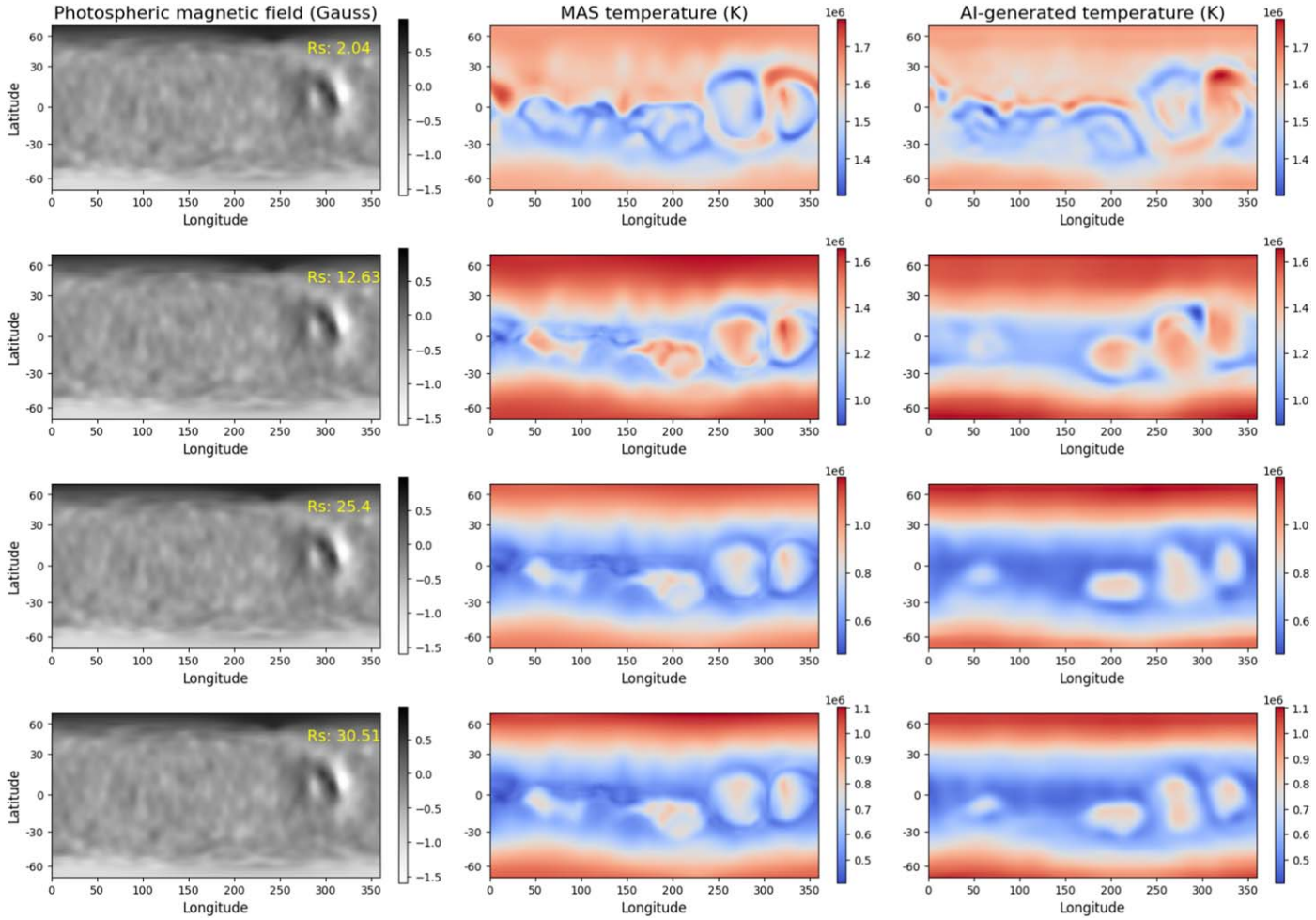

Figure 4. Comparison of solar coronal temperature maps between the MAS simulation results and AI-generated ones during CR 2220. Each column is the same as in Figures 2 and 3.

Adam (Kingma & Ba 2014) optimizer is used with the initial learning rate of 2×10^{-4}.

4. Results and Discussion

4.1. Qualitative Comparison

Figures 2, 3, and 4 represent three examples of image generation using the deep-learning models of the three parameters at distances of 2.04, 12.63, 25.40, and 30.51 solar radii, respectively. Figure 2 demonstrates a comparison of coronal magnetic fields between MAS simulation results and the AI-generated ones during CR 2194. Similarly, the comparison between the MAS simulation results and the AI-generated 3D radial velocity and temperature map during CR 2178 and CR 2220 is shown in Figures 3 and 4, respectively. We note that across a wide range of radial distances, the deep-learning models successfully generate the overall 3D structures and the complex nature of solar coronal dynamics. From the color bars of the middle and right columns of each figure, we observe that our deep-learning models can reproduce the topology and dynamics of the solar coronal parameters.

Next, we provide a comparison between the MAS simulation and AI-generated results of the parameters along the equator (0° latitude) of CR 2174 and CR 2220. The comparison is focused on two specific distances at 2.6 and 21.30 solar radii, which are shown in Figures 5 and 6, respectively. The active regions mostly appear at low-latitude regions (Linker et al. 1999), and the heliospheric current sheet is also produced at the solar magnetic equator (Desai et al. 2020); the parameters also show different properties in this region. At those distances, the solar parameters' behavior transitions from being primarily influenced by the solar magnetic field and coronal dynamics to being more affected by the interplanetary magnetic field and the dynamics of the heliosphere. In the first two rows of Figure 5, we observe that at a distance of 2.6 solar radii along the 0° latitude, the deep-learning models accurately generate the positions of the neutral line, as well as the positive and negative magnetic field values. The third and fourth rows display the AI-generated radial velocity profiles for both CRs, which closely resemble those obtained from the MAS simulation. The intensity plot in the last two rows in Figure 5 also shows consistency both in high- and low-temperature regions. However, certain errors occur at some positions of the AI-generated temperature maps. It is important to note that those errors can be attributed to the inherent limitations and uncertainties of our method. In Figure 6, the results at 21.30 solar radii demonstrate the consistent structure of parameters near the heliospheric regions. This consistency is particularly crucial because the interface between the coronal and

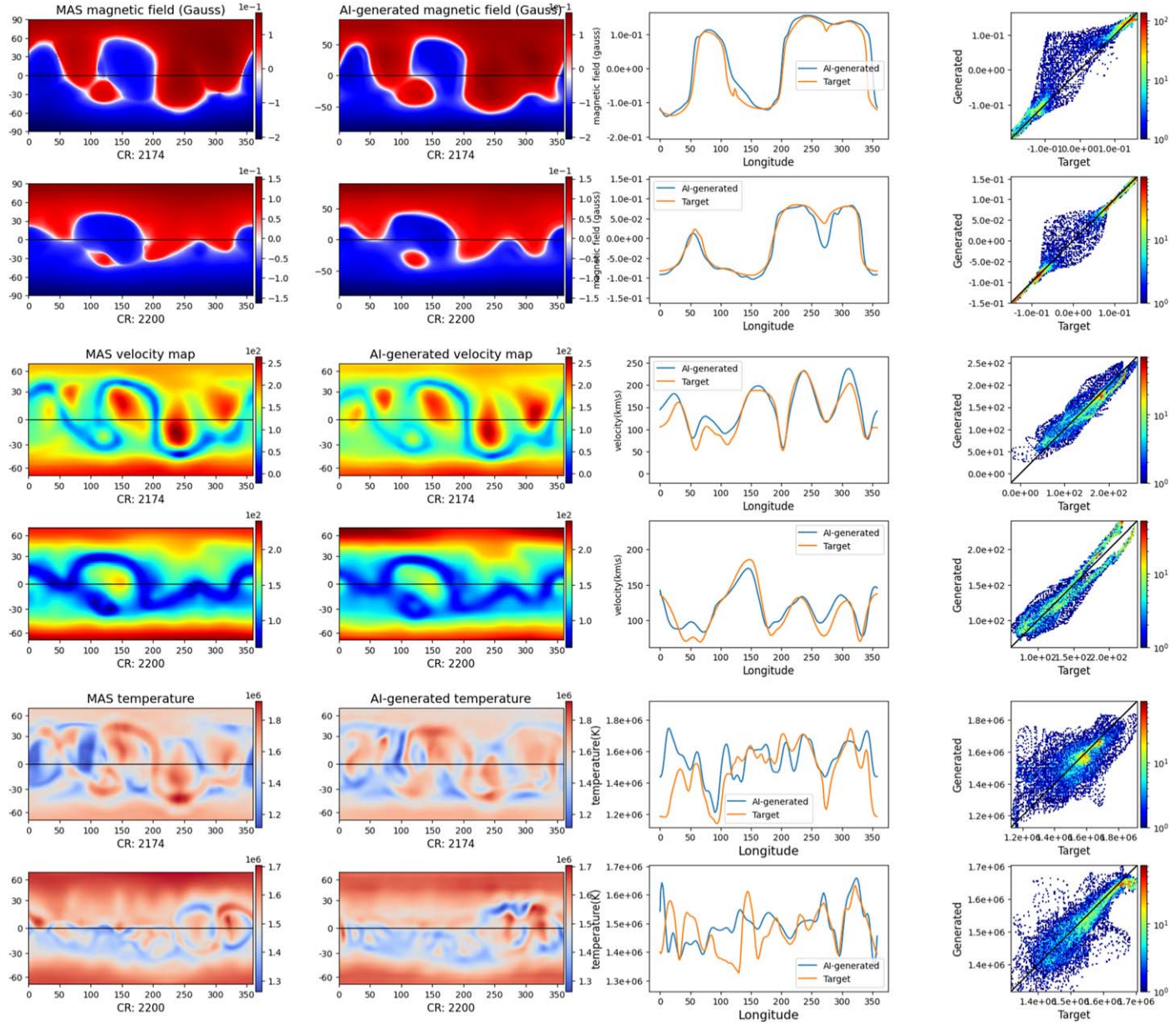

Figure 5. Two examples of comparisons of the MAS simulation results, which include the magnetic field, radial velocity, and temperature map plus AI-generated ones of the parameters along the equator (0° latitude) on CRs 2174 and 2220 at 2.6 solar radii. Left to right: MAS simulation results, AI-generated ones, the values of the three parameters at 0° latitude of CRs 2174 and 2220, and the 2D histograms, respectively.

heliospheric regions is typically situated in the supercritical-flow region, which is near 21.5 solar radii or 0.1 au (Linker 2011).

Next, we compare the MAS simulation and AI-generated results during the solar minimum (Figure 7) and solar maximum (Figure 8) periods at 21.30 solar radii. The comparisons in Figure 7 shows that the deep-learning models are able to reproduce the structure of the coronal parameters remarkably well during the solar minimum. It is shown that long-lived helmet streamers and coronal holes may persist over several solar rotations. Solar minimum conditions give us the opportunity to distinguish between the fundamental coronal structure and the solar active phenomena (Linker et al. 1999). This is not surprising as the match between the MAS simulation and the deep-learning models is poorer during high solar activity than at the solar minimum. The temporal variability of the photospheric magnetic field increases as the Sun approaches solar maximum (Riley et al. 2001). It is also noted that the synoptic map of the photospheric magnetic field largely affects the simulation results (Gressl et al. 2014).

4.2. Quantitative Comparison

The averaged pixel-to-pixel Pearson's CC (higher is better), normalized rms (NRMSE; smaller is better), and normalized mean absolute error (NMAE; smaller is better) values between those of the MAS simulation and the AI-generated values of the testing data set are calculated and presented in Table 1. Here, we calculate those three metrics for magnetic field, radial velocity, and temperature at specific heights (2.07, 8.22, 14.33, 21.30, and 26.42 solar radii). The additional CC loss

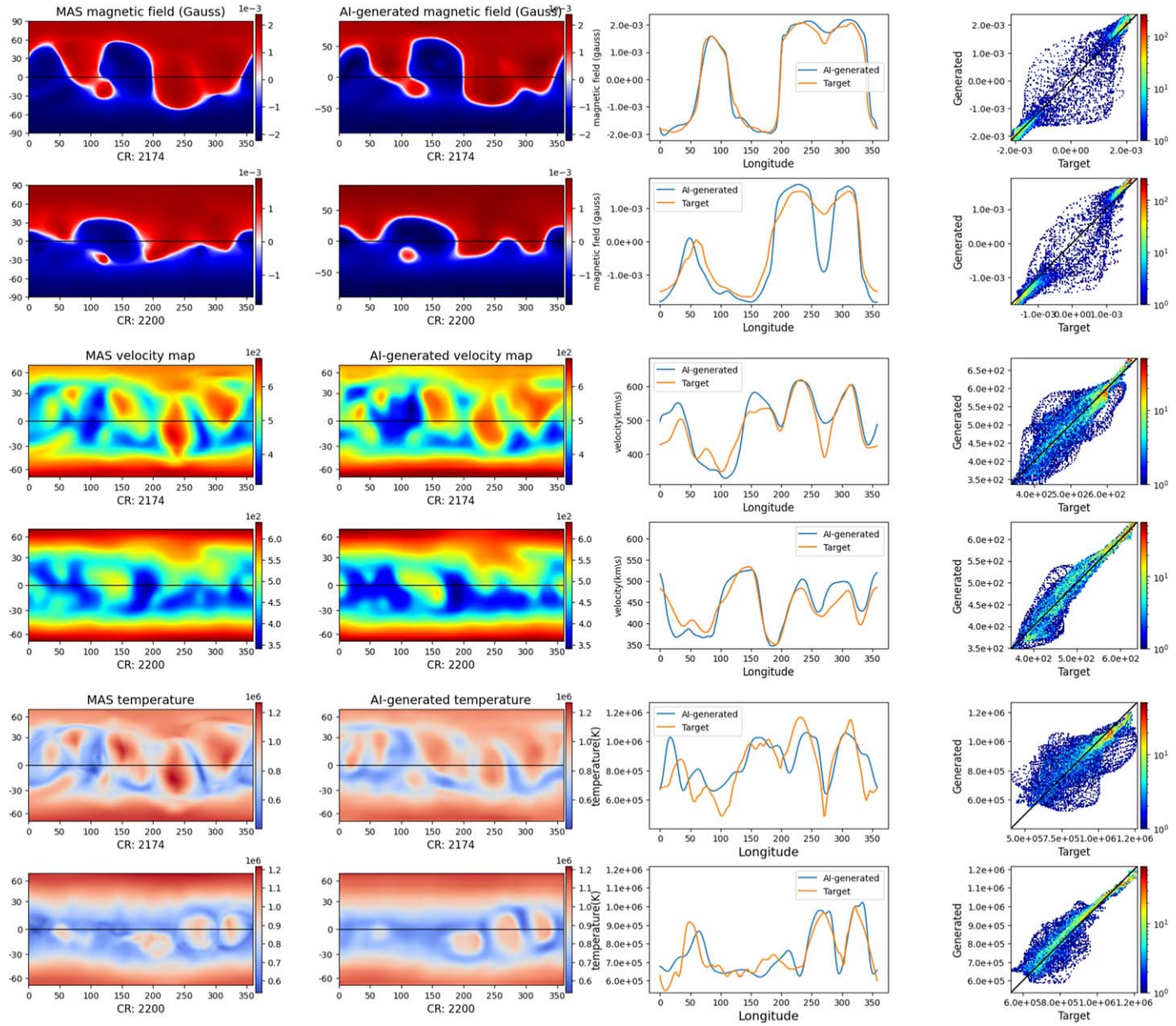

Figure 6. Comparisons of the MAS simulation results and AI-generated ones along the equator (0° latitude) during CRs 2174 and 2220 at 21.30 solar radii. The first column shows the MAS simulation results. The second column displays the corresponding AI-generated results for the magnetic field, radial velocity, and temperature, the third column shows the values of three parameters at 0° latitude of CRs 2174 and 2220, respectively, and the fourth column represents the 2D histograms.

function used in our deep-learning models has contributed to achieving higher CC values for the parameters not only in lower solar radii but also in higher solar radii. Furthermore, it is to be noted that the NRMSE and NMAE values of the magnetic field and the radial velocity are smaller compared to the temperature.

We use a single NVIDIA TITAN XP GPU, CUDA 11.4 and 12 GB, to train and test the 152 deep-learning models for each parameter. An AMD Ryzen 5 3600 6-core processor with a 16.0 GB RAM CPU is used for loading and preprocessing the data sets. Following our previous study (Rahman et al. 2023), the computing times for the parameters are much faster than the usual computational time on the MAS simulation (Caplan et al. 2019). For each parameter, it takes approximately 16 s to compute 152 deep-learning models of the test data set with a resolution of $182 \times 96 \times 152$ up to 30 solar radii.

5. Conclusion and Summary

In this study, we have applied Pix2PixCC models to generate the 3D structure of major solar coronal parameters from photospheric magnetic field data. We trained and tested 152 deep-learning models using a data set consisting of 169 pairs of CRs from 2010 June to 2023 February. The major findings of this study are summarized as follows. First, the Pix2PixCC models can efficiently and successfully generate the 3D solar coronal magnetic field, radial velocity, and temperature map with significantly high CC values. Such 3D structures of solar coronal parameters will be useful in analyzing solar observations and developing up-to-date models of the solar corona and inner heliosphere. Many multispectral properties of the corona observed in extreme ultraviolet and X-ray emission can be analyzed utilizing our AI-generated results along with our earlier AI-generated electron density results (Rahman et al. 2023).

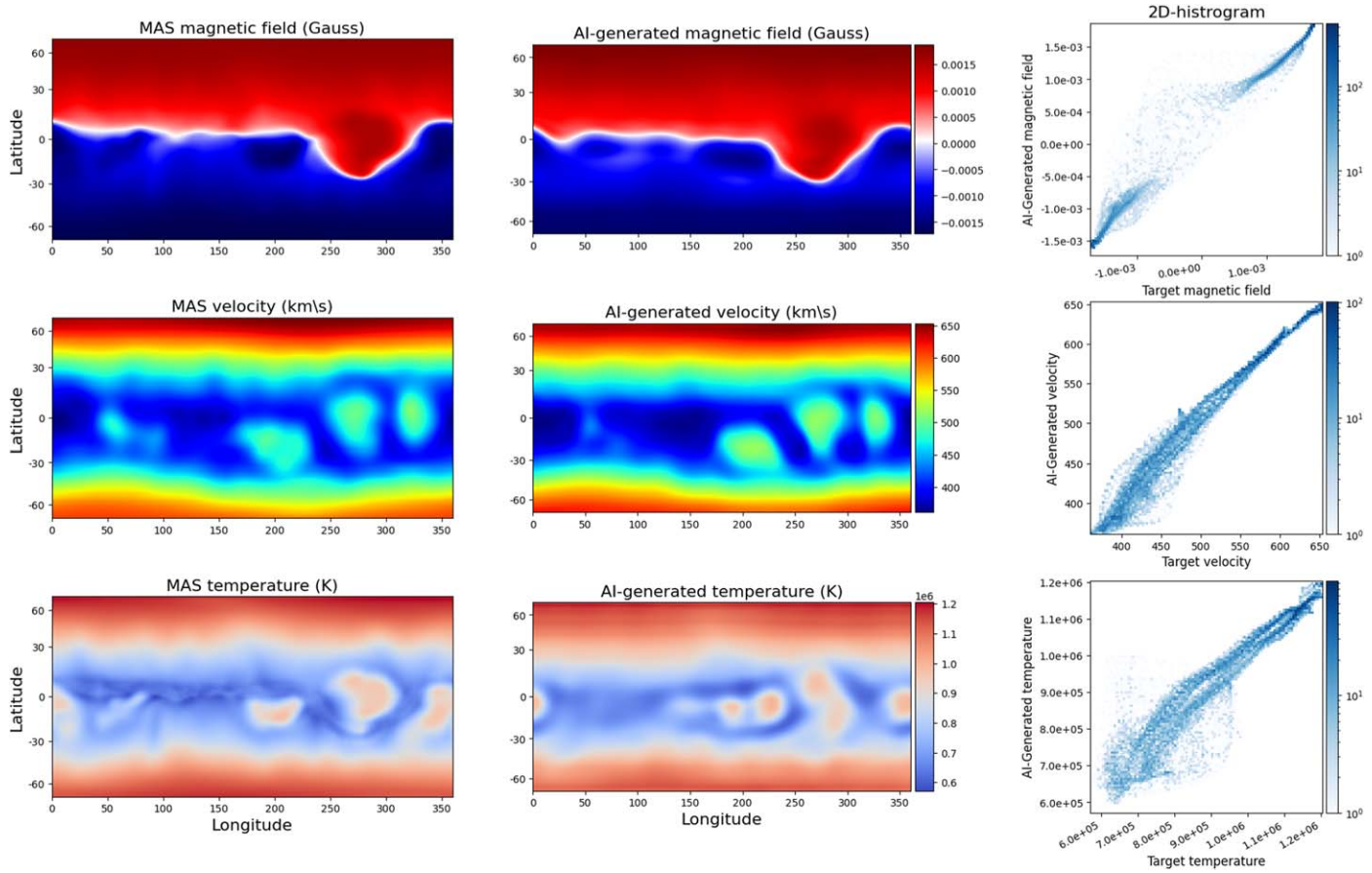

Figure 7. Comparisons between the MAS simulation results and AI-generated ones at a distance of 21.30 solar radii during a solar minimum period. From left to right the figure shows the MAS simulation results (left), AI-generated ones (middle), and the 2D histograms between the target and AI-generated ones (right) on CR 2224 (2019 December 10).

Table 1
The Pearson's Correlation Coefficient (CC), Normalized rms Error (NRMSE), and Normalized Mean Absolute Error (NMAE) between AI-generated Data and Target Values for the Testing Data Set

Solar Radius	Magnetic Field (G)			Velocity (km s^{-1})			Temperature (K)		
	CC	NRMSE	NMAE	CC	NRMSE	NMAE	CC	NRMSE	NMAE
2.07	0.99	0.10	0.06	0.98	0.09	0.16	0.99	0.13	0.09
8.22	0.98	0.13	0.08	0.99	0.08	0.14	0.98	0.17	0.11
14.33	0.99	0.14	0.09	0.98	0.07	0.13	0.98	0.16	0.11
21.30	0.99	0.14	0.08	0.99	0.08	0.13	0.99	0.18	0.12
26.42	0.98	0.12	0.09	0.99	0.08	0.15	0.99	0.16	0.11

Second, our study also demonstrates good consistency between the MAS simulation and AI-generated results in the solar equatorial region at 2.6 and 21.30 solar radii. As we know, most heliospheric models like the Wang–Sheeley–Arge model (Arge et al. 2004) have inputted boundary conditions as data at 21.5 solar radii (0.1 au). Third, while the AI-generated results during the solar minimum period agree well with the MAS ones for three coronal parameters, those during the solar maximum period have some inconsistencies, especially for temperature. Finally, the evaluation metrics show high CC values and low NRMSE and NMAE values for both low and high solar radii. The overall computational time required for testing the 152 models for both parameters is significantly shorter compared to the MAS simulation.

As the MAS simulation is a regularization model, we may effectively reduce the simulation time by using our results together with the electron density results obtained from our prior study (Rahman et al. 2023) as an initial configuration to obtain an equilibrium condition. The AI-generated results can be potentially used for specifying the condition on global magnetohydrodynamic models to reproduce large-scale coronal phenomena, heliospheric structures, and solar wind modeling. The ambient solar coronal parameter structures can be applied for the near-real-time forecasting of the heliospheric propagation of solar eruptions. In the future, we plan to predict heliospheric parameters from 21.5 solar radii (0.1 au) to 1 au and compare our deep-learning model results with the MAS heliospheric models (Lionello et al. 2009), the Wang–Sheeley–

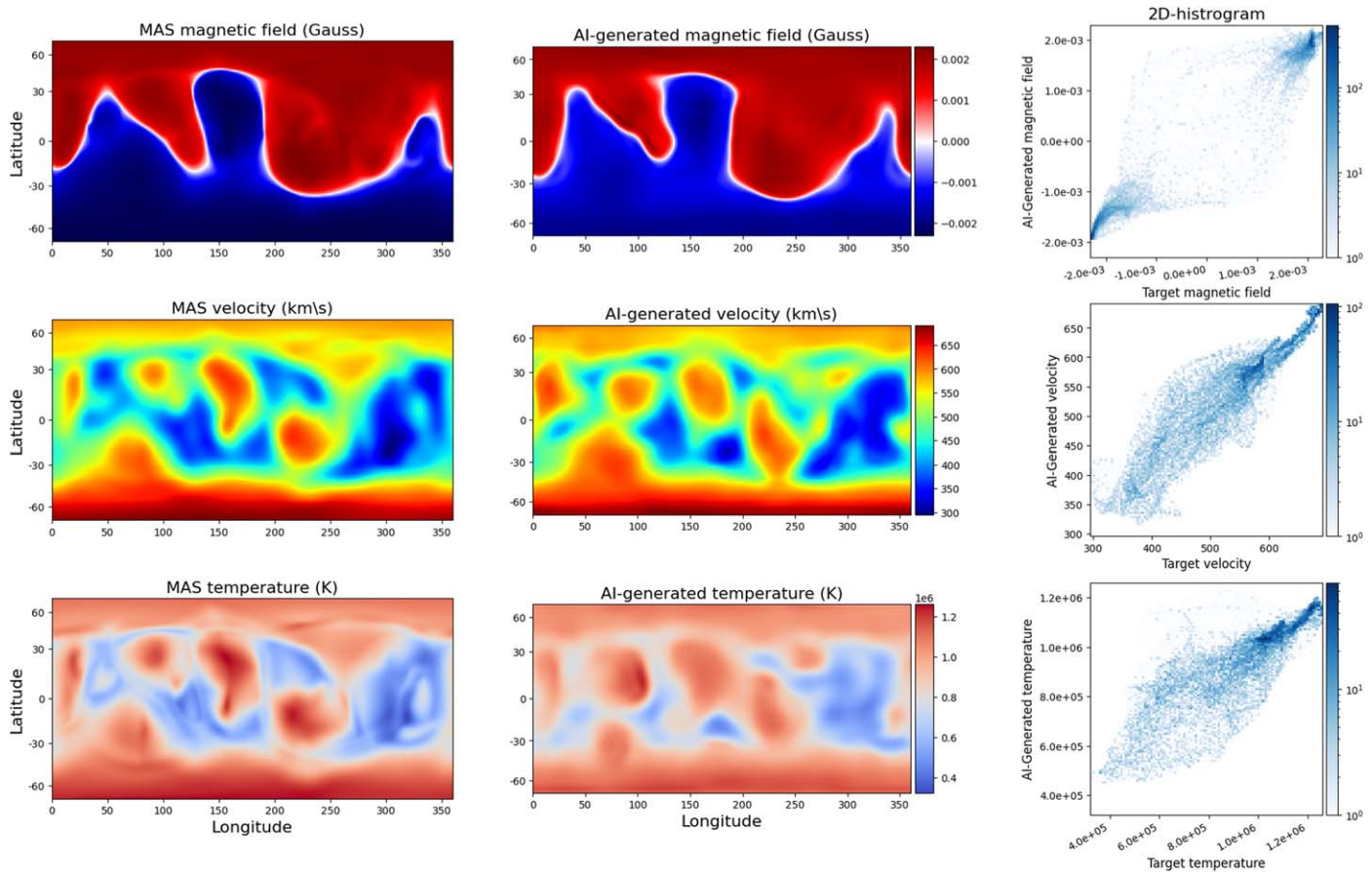

Figure 8. Comparisons between the MAS simulation results and AI-generated ones at 21.30 solar radii during a solar maximum period. From left to right the figure shows the MAS simulation results, AI-generated ones, and the 2D histograms between the target and AI-generated ones during CR 2170 (2015 November 28).

Arge model (Arge et al. 2004), and recently published deep-learning base model (Son et al. 2023). Furthermore, we will compare our AI-generated results with observations (e.g: Bemporad 2017; Cho et al. 2018).

Acknowledgments

This research was supported by a Basic Science Research Program through the National Research Foundation of Korea (NRF) funded by the Ministry of Education (RS-2023-00248916), the Korea Astronomy and Space Science Institute under the R&D program (Project No. 2024-1-850-07) supervised by the Ministry of Science and ICT (MSIT), and an Institute of Information & Communications Technology Planning & Evaluation (IITP) grant funded by the Korean government (MSIT) (No. RS-2023-00234488, Development of solar synoptic magnetograms using deep learning, 15%). We thank the numerous team members who have contributed to the MAS simulation. We acknowledge the community effort devoted to developing the following open-source packages used in this work.

Software: PyTorch (Paszke et al. 2019), NumPy (Harris et al. 2020), Matplotlib (Hunter 2007), Skimage (Van der Walt et al. 2014), SunPy (The SunPy Community et al. 2020).

ORCID iDs

Sumiaya Rahman https://orcid.org/0009-0004-9329-9474
Hyun-Jin Jeong https://orcid.org/0000-0003-4616-947X
Ashraf Siddique https://orcid.org/0000-0003-2186-5735
Yong-Jae Moon https://orcid.org/0000-0001-6216-6944
Bendict Lawrance https://orcid.org/0000-0001-6648-0500

References

Arge, C., Luhmann, J., Odstrcil, D., et al. 2004, JASTP, 66, 1295
Bemporad, A. 2017, ApJ, 846, 86
Caplan, R. M., Linker, J. A., Mikić, Z., et al. 2019, JPhCS, 1225, 012012
Cho, I.-H., Moon, Y.-J., Nakariakov, V. M., et al. 2018, PhRvL, 121, 075101
Desai, R. T., Zhang, H., Davies, E. E., et al. 2020, SoPh, 295, 130
Goodfellow, I. J., Pouget-Abadie, J., Mirza, M., et al. 2014, arXiv:1406.2661
Gressl, C., Veronig, A. M., Temmer, M., et al. 2014, SoPh, 289, 1783
Harris, C. R., Millman, K. J., Van Der Walt, S. J., et al. 2020, Natur, 585, 357
Hunter, J. D. 2007, CSE, 9, 90
Isola, P., Zhu, J.-Y., Tinghui, E., et al. 2017, in 2017 IEEE Conf. on Computer Vision and Pattern Recognition (Piscataway, NJ: IEEE), 5967
Jang, S., Kwon, R.-Y., Linker, J. A., et al. 2021, ApJL, 920, L30
Jeong, H.-J., Moon, Y.-J., Park, E., et al. 2020, ApJL, 903, L25
Jeong, H.-J., Moon, Y.-J., Park, E., et al. 2022, ApJS, 262, 50
Jia, P., Huang, Y., Cai, B., et al. 2019, ApJL, 881, L30
Kaiser, M. L., Kucera, T. A., Davila, J. M., et al. 2008, SSRv, 136, 5
Kim, T., Park, E., Lee, H., et al. 2019, NatAs, 3, 397
Kingma, D. P., & Ba, J. 2014, arXiv:1412.6980
Lawrance, B., Lee, H., Park, E., et al. 2022, ApJ, 937, 111
Linker, J. A. 2011, A Next-Generation Model of the Corona and SolarWind: Final Report AFRL-OSR-VA-TR-2012-0199, Predictive Science Inc., https://apps.dtic.mil/sti/tr/pdf/ADA563658.pdf
Linker, J. A., Mikić, Z., Biesecker, D. A., et al. 1999, JGR, 104, 9809
Linker, J. A. 1998, Global Magnetohydrodynamic Modeling of the Solar Corona, Contractor Report 19980107903, Science Applications International Corporation, https://ntrs.nasa.gov/citations/19980107903
Lionello, R., Linker, J. A., & Mikić, Z. 2009, ApJ, 690, 902
Mao, Y., Zang, J., & Letaief, K. B. 2016, IJSAC, 34, 3590
Mikić, Z., Downs, C., Linker, J., et al. 2018, NatAs, 2, 913

Mikić, Z., Linker, J. A., Schnack, D. D., et al. 1999, PhPl, 6, 2217
Park, E., Moon, Y.-J., Lee, J.-Y., et al. 2019, ApJL, 884, L23
Park, E., Moon, Y.-J., Lim, Daye, et al. 2020, ApJL, 891, L4
Paszke, A., Gross, S., Massa, F., et al. 2019, Advances in Neural Information Processing Systems 32, ed. H. Wallach et al. (NeurIPS), https://papers.nips.cc/paper_files/paper/2019/hash/bdbca288fee7f92f2bfa9f7012727740-Abstract.html
Pesnell, W. D., Thompson, B. J., & Chamberlin, P. C. 2012, SoPh, 275, 3
Rahman, S., Moon, Y.-J., Park, E., et al. 2020, ApJL, 897, L32
Rahman, S., Shin, S., Jeong, H.-j., et al. 2023, ApJ, 948, 21
Riley, P., Linker, J., Mikić, Z., et al. 2001, Space Weather (Washington, DC: American Geophysical Union), 159
Riley, P., Lionello, R., Linker, J., et al. 2011, SoPh, 274, 361
Shin, G., Moon, Y.-J., Park, E., et al. 2020, ApJL, 895, L16
Shorten, C., & Khoshgoftaar, T. M. 2019, J. Big Data, 6, 1
Son, J., Sung, S.-K., Moon, Y.-J., et al. 2023, ApJS, 267, 45
Tan, B. 2022, RAA, 22, 072001
The SunPy Community, Barnes, W. T., Bobra, M. G., et al. 2020, ApJ, 890, 68
Van der Walt, S., Schönberger, J. L., Nunez-Iglesias, J., et al. 2014, PeerJ, 2, e453
Wang, T.-c., Liu, M.-Y., Jun-Yan, T., et al. 2018, in Proc. of the IEEE Conf. on Computer Vision and Pattern Recognition (Los Alamitos, CA: IEEE Computer Society), 8798